# Janus $NiN_4$-$CuN_4$ Catalyst Supported by Double-layered ZIF-8 Structure for Electrocatalytic $CO_2$ Reduction to $C_{2+}$ Products

*Gege Zhang[1], Qianyun Tan[1], Xiaoyu Xu[1], Faqian Liu[1*]*

*1School of Chemical Engineering and Technology, Sun Yat-sen University, Zhuhai 519082, China*

## S1 Characterization

The morphology of the synthesized catalyst was observed using field emission scanning electron microscopy (FESEM, Axia ChemiSEM HiVac) and high-resolution transmission electron microscopy (HR-TEM, JEOLJEM-F200 (URP)) equipped with energy-dispersive X-ray spectroscopy (EDS). High-angle annular dark-field scanning transmission electron microscopy (HAADF-STM) images was viewed by JEOLJEM-F200 (URP). The crystal structure of the prepared catalyst was analyzed using X-ray diffraction patterns (XRD). XRD was performed on D/MAX2200 Rigaku at a scanning speed of 10° $min^{-1}$ and a scanning range of 0-90°. Subsequent to a degassing procedure lasting 4 hours at 473 K, the N2 adsorption-desorption isotherm was conducted on Micromeritics 113 ASAP 2460. X-ray photoelectron spectroscopy (XPS) was tested on X-ray photoelectron spectrometer (Thermo Fisher/ESCALAB QXi). The Raman spectroscopy was conducted using a Raman spectrometer (Renishaw inVia Raman microscope). In situ Raman spectroscopy is utilized to monitor the intermediate states of electrocatalytic processes. The concentration of metal ions in the catalyst was determined by inductively coupled plasma-optical emission spectrometer (ICP-OES, Agilent ICP-OES 730).

## S2 Computational Methods

All spin-polarized density functional theory (DFT) calculations were performed using the ABACUS package[1, 2], which employs a linear combination of atomic orbitals (LCAO) framework. The exchange–correlation interactions were described within the generalized gradient approximation (GGA) using the Perdew–Burke–Ernzerhof (PBE) functional. The interaction between valence electrons and ionic cores was treated using norm-conserving pseudopotentials. The PBE exchange–correlation functional was employed together with DFT-D3(BJ) dispersion corrections. Brillouin-zone sampling used a 3 × 3 × 3 k-point mesh, and a real-space/FFT grid cutoff of 100 Ry was applied. Structural optimizations were carried out until the residual force on each atom was less than 0.02 eV Å−1, with the total energy convergence threshold set to 10−6 eV. Brillouin zone integrations were performed using the Monkhorst–Pack scheme with a 2×2×1 k-point mesh. The free energy profiles of the CO2 electroreduction reaction were evaluated using the computational hydrogen electrode (CHE) model, in which the reaction free energy change is expressed as:

$$\Delta G = \Delta E + \Delta E_{ZPE} - T\Delta S + \Delta G_{pH} + \Delta G_U$$
$$\Delta G_{pH} = pH \times k_B T \ln 10$$

where ΔE is the binding energy of adsorbed species, ΔE_ZPE is the zero-point energy, ΔS is the entropy change of the system, T is the temperature (298.15 K), ΔG_pH is the pH correction term, and $\Delta G_u$ is the contribution from the electrode potential to ΔG.

## S3 Synthesis of $NiN_4$/$CuN_4$

A solution of 0.357 g $NiCl_2 \cdot 6H_2O$ and 0.743 g 1,10-phenanthroline in 120 mL methanol was prepared and stirred for 0.5 h. Subsequently, 4.61 g $Zn(CH_3COO)_2 \cdot 2H_2O$ was added to the solution and stirred for 1 h. The aforementioned solution was then added dropwise to a solution of 17.2 g 2-MeIm in 10 mL of methanol, which was stirred for 5 min and allowed to precipitate for 24 h. The products were washed with methanol, centrifuged three times and then dried in a vacuum at 60 °C. 250 mg Niphen@ZIF-8 was heated to 900 °C under $N_2$ in a tube furnace at 5 °C/min and held for 2 h. After cooling, black Ni-N-C, was collected. The product was prepared and named Cu-N-C were obtained by replacing 0.357 g $NiCl_2 \cdot 6H_2O$ with 0.256 g $CuCl_2 \cdot 2H_2O$, and other steps were the same

as in the preparation of Ni-N-C. 250 mg of Ni-N-C and Cu-N-C were add to 50 mL of EtOH, ultrasound 15 min, centrifuged and dried in a vacuum at 60 °C.

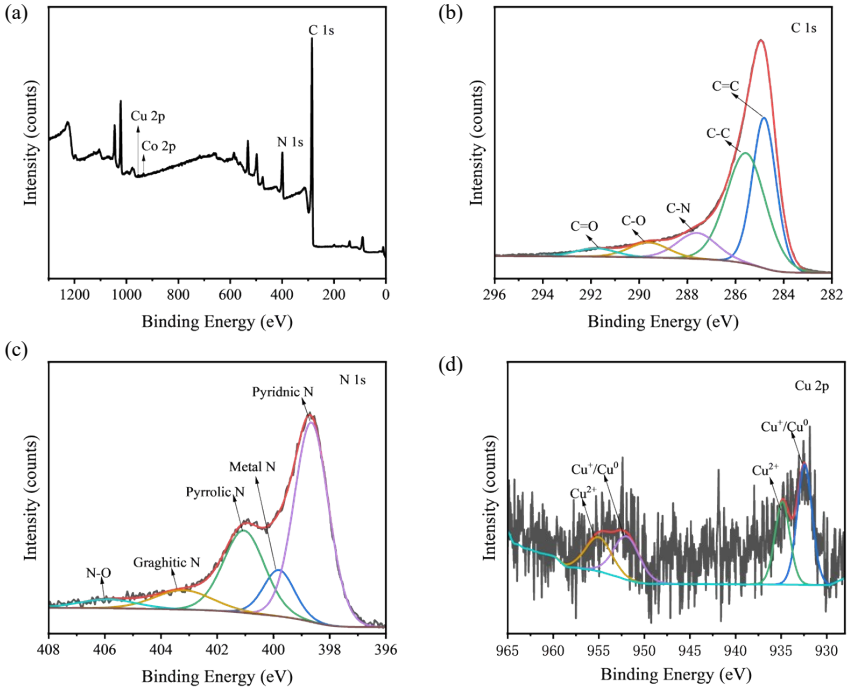


**Figure S1.** (a) The XPS survey of $CoN_4@CuN_4$, (b) the C1s spectra of $CoN_4@CuN_4$, (c) the N1s spectra of $CoN_4@CuN_4$, and (d) the Cu2p spectra of $CoN_4@CuN_4$.

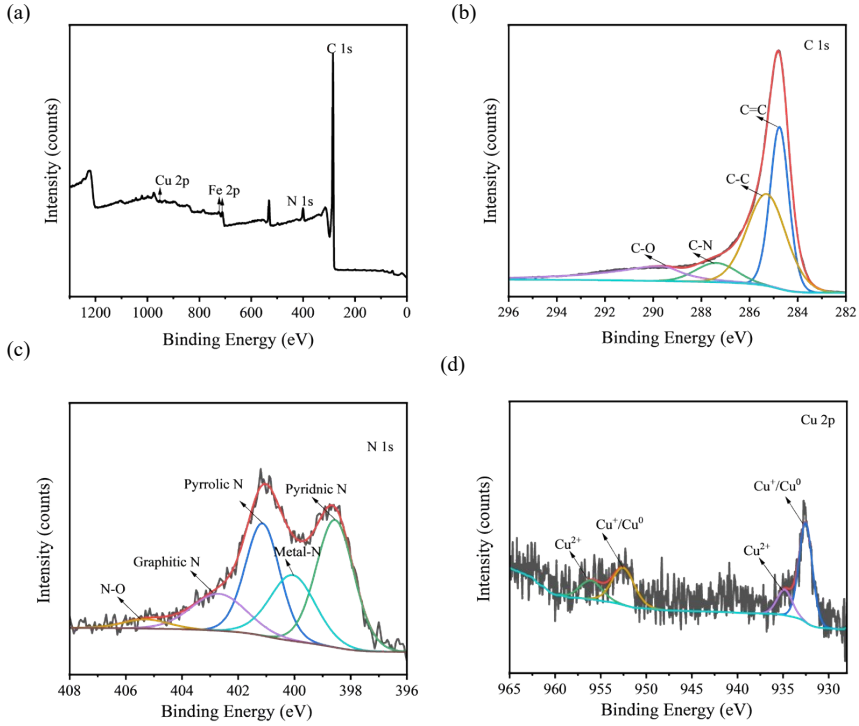


Figure S2. (a) The XPS survey of $FeN_4@CuN_4$, (b) the C1s spectra of $FeN_4@CuN_4$, (c) the N1s spectra of $FeN_4@CuN_4$, and (d) the Cu2p spectra of $FeN_4@CuN_4$.

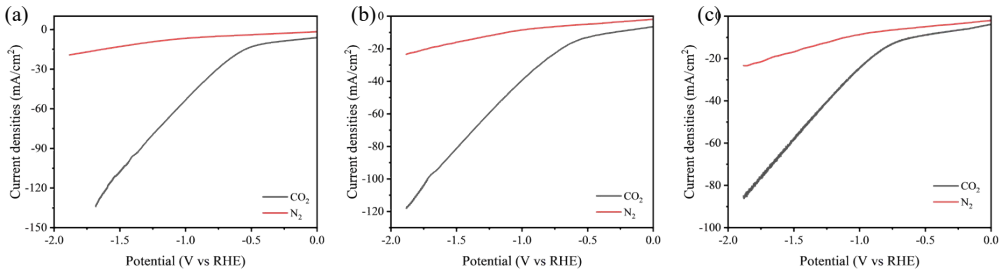


Figure S3. The LSV curves of (a) $NiN_4$@$CuN_4$, (b) $FeN_4$@$CuN_4$ and (c) $CoN_4$@$CuN_4$ in $N_2$ or $CO_2$ atmosphere.

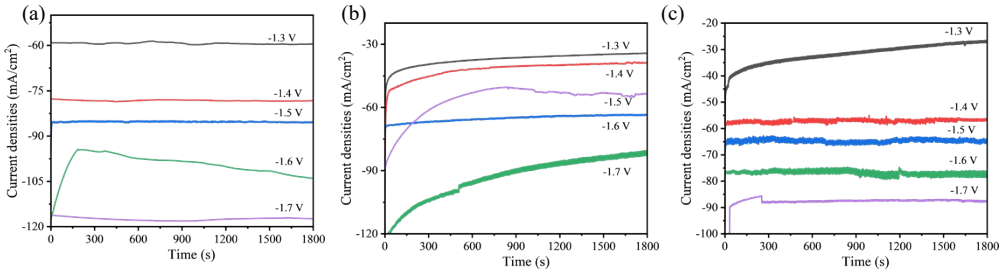


**Figure S4.** The it curves of (a) $NiN_4$@$CuN_4$, (b) $FeN_4$@$CuN_4$ and (c) $CoN_4$@$CuN_4$ in different potential.

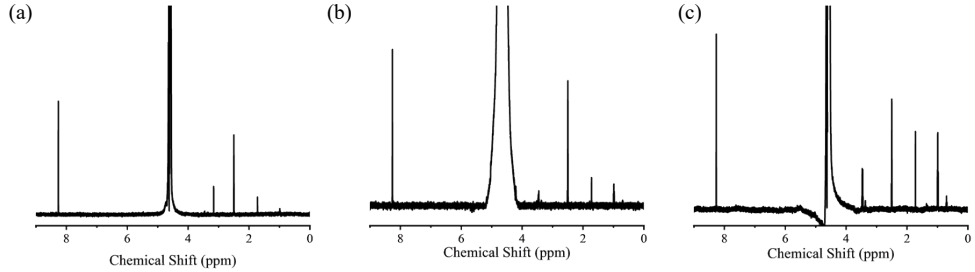


Figure S5. The $^1$H NMR spectra of (a) $FeN_4$@$CuN_4$, (b) $CoN_4$@$CuN_4$ and (c) $NiN_4$@$CuN_4$.

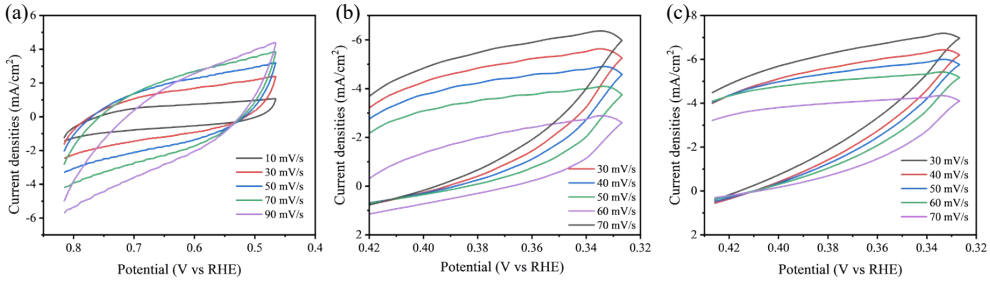


Figure S6. The CV curves of (a) $NiN_4$@$CuN_4$, (b) $FeN_4$@$CuN_4$ and (c) $CoN_4$@$CuN_4$ at different scan rate.

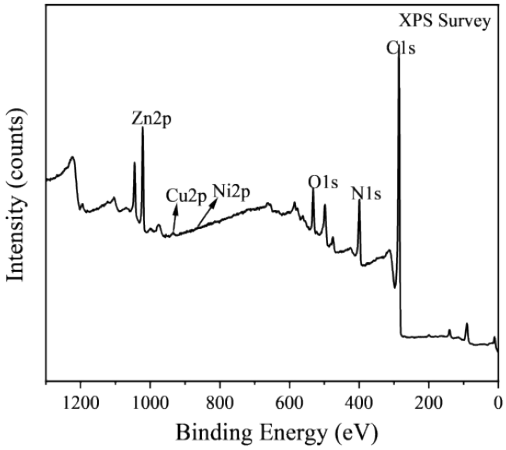


Figure S7. The XPS survey of $NiN_4@CuN_4$.

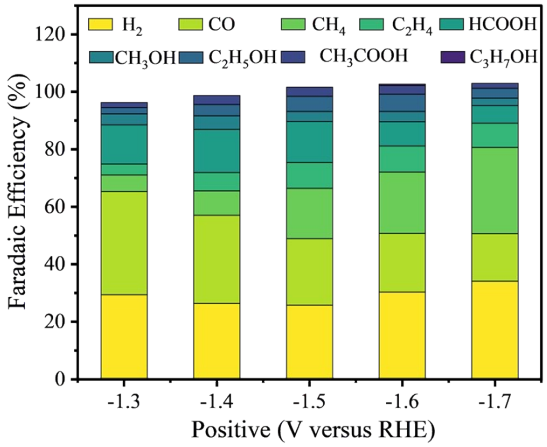


Figure S8. FE of electrocatalytic products for $NiN_4/CuN_4$.

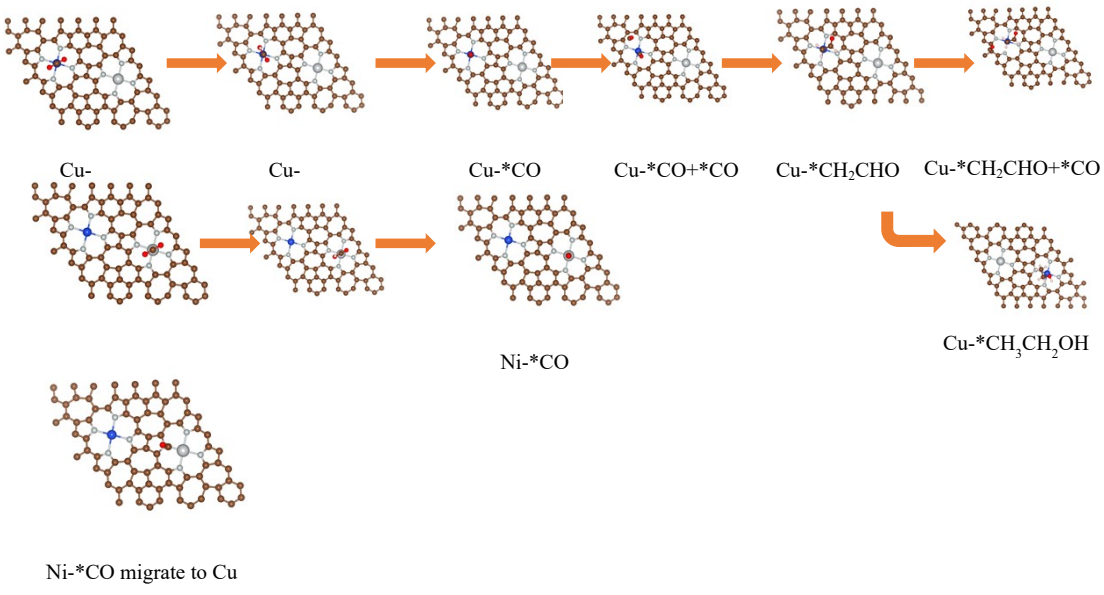


Figure S9. The pathway of $CO_2RR$ for $NiN_4@CuN_4$.

Table S1. The metal elements content of $FeN_4$@$CuN_4$ $CoN_4$@$CuN_4$ and $NiN_4$@$CuN_4$ by ICP-OES.

| | Cu (wt%) | Fe (wt%) | Co (wt%) | Ni (wt%) |
|---|---|---|---|---|
| $FeN_4$@$CuN_4$ | 0.79 | 3.21 | ---- | ---- |
| $CoN_4$@$CuN_4$ | 0.94 | ---- | 1.81 | ---- |
| $NiN_4$@$CuN_4$ | 1.68 | ---- | ---- | 2.32 |

Table S2. Comparison of the $CO_2$RR activity for $C_{2+}$ between the $NiN_4$@$CuN_4$ catalyst with other reported Cu catalysts under the basic condition in the literature.

| Catalysts | FE($C_{2+}$) | Electrolyzer | E(V vs RHE) | Electrolyte | Reference |
|---|---|---|---|---|---|
| $Cu_2S_{1-x}$ | 73.3% | flow cell | -0.3 | 0.5 M $KHCO_3$ | 3 |
| Ag-Cu | 80.2% | flow cell | -1 | 3 M KOH | 4 |
| $Cu_{0.9}Zn_{0.1}$ | 91% | flow cell | -1.1 | $H_2SO_4$+3 M KCl | 5 |
| Cu cube/CN | 49.6% | H cell | -1.15 | 0.1 M $KHCO_3$ | 6 |
| OD-$La_{0.10}$-$CuO_x$ | 80% | flow cell | -1.37 | 1M KCl | 7 |
| Cu-PCNF@O2 | 70.7% | flow cell | -2.2 | 1 M KOH | 8 |
| UC-Cu-BTEC-2 | 72.5% | flow cell | -2.7 | 1 M $KHCO_3$ | 9 |
| $NiN_4$@$CuN_4$ | 81.0% | flow cell | -1.6 | 1 M KOH | This work |

## References


1. P. Li, X. Liu, M. Chen, P. Lin, X. Ren, L. Lin, C. Yang and L. He, *Computational Materials Science*, 2016, **112**, 503-517.
2. M. Chen, G. C. Guo and L. He, *Journal of Physics: Condensed Matter*, 2010, **22**, 445501.
3. C. Guo, Y. Guo, Y. Shi, X. Lan, Y. Wang, Y. Yu and B. Zhang, *Angewandte Chemie International Edition*, 2022, **61**.
4. Z. Cai, N. Cao, F. Zhang, X. Lv, K. Wang, Y. He, Y. Shi, H. Bin Wu and P. Xie, *Applied Catalysis B: Environmental*, 2023, **325**, 122310.
5. J. Zhang, C. Guo, S. Fang, X. Zhao, L. Li, H. Jiang, Z. Liu, Z. Fan, W. Xu, J. Xiao and M. Zhong, *Nature Communications*, 2023, **14**, 1298.
6. N. Zhang and Y. Zhang, *Chemical Engineering Journal*, 2024, **499**, 156694.

7. Z. Guo, H. Zhu, Z. Yan, L. Lei, D. Wang, Z. Xi, Y. Lian, J. Yu, K. L. Fow, H. Do, J. D. Hirst, T. Wu and M. Xu, *Applied Catalysis B: Environment and Energy*, 2025, **364**, 124839.
8. X. Jiang, Y. Zhao, Y. Kong, J. Sun, S. Feng, Q. Hu, H. Yang and C. He, *Chinese Journal of Catalysis*, 2024, **58**, 216-225.
9. B. A, X. Jin, M. Wang, Y. Wang, W. Chen, Z. Wei, Z. Du, X. Liu, Y. Wang and L. Zhang, *Chemical Engineering Journal*, 2024, **500**, 157076.